Exergetic and economic evaluation of a novel integrated system for trigeneration of power, refrigeration and freshwater using energy recovery in natural gas pressure reduction stations

Hooman Golchoobian[1] · Seyfolah Saedodin[1] · Bahram Ghorbani[2]

Abstract

Nowadays, with increasing energy consumption, global warming, and many problems caused by weather conditions, the tendency to use novel methods of energy generation with high efficiency and low cost that reduce environmental pollution has increased. This study investigates the feasibility of using gas pressure energy recovery in natural gas pressure reduction stations by turboexpanders for cogeneration of power and refrigeration. Turboexpanders and compression refrigeration cycles are employed to recover the energy from natural gas pressure reduction stations. Then, natural gas along with the compressed air enters the Brayton power generation cycle and its waste heat is used in the carbon dioxide (CO_2) power generation plant, multistage Rankine cycle, and multi-effect thermal desalination unit. This integrated structure generates 105.6 MW of power, 2.960 MW of refrigeration, and 34.73 kg s^{-1} of freshwater. The electrical efficiencies of the Rankine power generation cycle, CO_2 power generation plant, and the whole integrated structure are 0.4101, 0.4120, and 0.4704, respectively. The exergy efficiency and irreversibility of the developed integrated structure are 60.59% and 68.17 MW, respectively. The exergy analysis of the integrated structure shows that the highest rates of exergy destruction are related to the combustion chamber (59.68%), heat exchangers (14.70%), and compressors (14.46%). The annualized cost of the system (ACS) is used to evaluate the developed hybrid system. The economic analysis of the integrated structure indicated the period of return, the prime cost of the product, and capital cost are 2.565 years, 0.0430 US\$ kWh^{-1}, and 372.3 MMUS\$, respectively. The results reveal that the period of return is highly sensitive to the electricity price, such that the period of return in the developed integrated structure is less than 5 years for the electricity price of 0.092 US\$ kWh^{-1} and more. Also, the period of return is less than 5 years for the initial investment cost of 632.9 MMUS\$ and less, which is economically viable.

Keywords Gas pressure reduction stations · Trigeneration system · Rankine power generation cycle · CO_2 power plant · Multi-effect desalination unit · Exergy and economic analyses

List of symbols

E	Specific flow exergy (kJ kmol^{-1})
Ex	Exergy (kW)
$\dot{m}$	Mass flow rate (kg s^{-1})
H	Enthalpy (kJ kmol^{-1})
P	Pressure (kPa)
T	Temperature (°C)
W	Work (kW)
S	Entropy (kJ kmol^{-1} °C^{-1})

Greek letters

η	Efficiency
Σ	Sum
$\int$	Integration

Subscripts

C	Cold
H	Hot
I	Inlet
O	Outlet
Id	Ideal
Ph	Physical
Ch	Chemical
T	Total
acap	Annualized capital cost
Cap	Capital cost
amain	Annualized maintenance cost

✉ Hooman Golchoobian
  h.golchoobian@gmail.com

1 Faculty of Mechanical Engineering, Semnan University, Semnan, Iran

2 Faculty of Engineering Modern Technologies, Amol University of Special Modern Technologies, Amol, Iran

Main   Maintenance cost
aope   Annualized operating cost

Superscript
P   Pressure component
T   Thermal component

Abbreviations
CGSs   City gate stations
LNG   Liquefied natural gas
MED-TVC   Multi-effect distillation-thermal vapor
              compression
SRA   Structured retrofitting approach
HRSG   Heat recovery system generator
MED   Multi-effect desalination
CO_2 Carbon dioxide
CRF   Capital Recovery Factor
ACS   Annualized cost of system
Ope   Operating cost
arep   Annualized replacement cost
Rep   Replacement cost
(LCOE)   Levelized cost of energy
ORC   Organic Rankine cycle

Names used for blocks in plants
Ti   Turbine
CCi   Combustion chamber
Vi   Valve
Ci   Compressor
HXi   Heat exchanger
Si   Flash drum

Introduction

Turboexpanders are devices for converting the compressed gas energy to mechanical power through a pressure reduction process. These devices are employed to prevent energy loss in natural gas pressure reduction stations and are proposed as an alternative to pressure relief valves (PRVs) used in these stations. Turboexpanders convert the gas pressure energy to mechanical or electrical power using a generator by reducing the gas pressure to the desired value for delivery to the consumer. Process integration increases efficiency and decreases the number of equipment applied in the integrated system. Therefore, many researchers have focused on the integrated structures to exploit the waste energy in pressure reduction stations [1]. Deymi-Dashtebayaz et al. [2] developed and analyzed a novel integrated system for cogeneration of power and freshwater in city gate stations (CGSs). They used a turboexpander to recover the energy of the pressure drop at the station and a multi-effect distillation-thermal vapor compression (MED-TVC) system to produce freshwater. The heat required for the turboexpander and desalination

system was supplied by the waste heat of the pressure reduction station. A model was developed to evaluate the system efficiency of three stations with different capacities and the effective thermodynamic and performance parameters were optimized using a multiobjective optimization method. Yao et al. [3] investigated the pressure loss recovery in gas pressure reduction stations by a power generation system. They also examined the turbine inlet flow rate and isentropic efficiency. The results illustrated that the novel hybrid system generated 147 kWh of power in a typical day. The system energy and exergy efficiencies were calculated as 96.09% and 66%, respectively. Lo Casio et al. [4] presented a new structured retrofitting approach (SRA) to be used in gas pressure reduction stations by a turboexpander. A mathematical model was developed to minimize the levelized cost of energy (LCOE). The model was solved by different methods and tested for different thermal loads, fuel costs, and gas flow rates. The proposed optimization technique in gas pressure reduction stations provided the best integrated structure in turboexpander technology. Li et al. [5] proposed a hybrid system to exploit the energy of the natural gas pressure reduction and low-grade waste heat by the Rankine cycle. They optimized the thermodynamic and economic parameters of the system by modeling and using a multiobjective optimization method. By comparing the proposed hybrid system with the non-hybrid system, they found that energy and exergy efficiencies increased by about 17% and 22%, respectively, and the cost of electrical energy was reduced by about 42%. Pajączek et al. [6] investigated the natural gas liquefaction using pressure changes in gas pressure reduction stations. They developed and tested a novel hybrid structure that supplied energy to the natural gas liquefaction unit using a turboexpander in the gas pressure reduction station. The analyses were performed on a specific gas pressure reduction station with three configurations and two types of turboexpanders integrated with natural gas liquefaction units with 6 different sizes. Energy and exergy efficiencies of the hybrid systems varied from 35.40% to 66.64% and 15.75% to 46.33%, respectively, based on the size and gas liquefaction method, which indicated the thermo-ecological costs of LNG production reduced by 8.2%. Golchoobian et al. [7] developed a novel hybrid unit of turboexpander and compression refrigeration cycle for the gas pressure reduction station of a power plant. They examined the system's potential for generating electric and cooling power over a period of several months, taking into account changes in station performance parameters and environmental conditions. The generated net power output and cooling were about 950 kW and 2700–5300 kW, respectively. Diao et al. [8] designed and applied a two-stage oil-free screw expander in a CGS. The critical speeds of the rotors, seals, and bearings were investigated. The results depicted that the designed system was much simpler than the conventional expanders used in

CGSs and lacked their sealing and bearing selection challenges. Also, the stable performance of this type of expanders proved the feasibility and ease of using them for energy recovery from high natural gas pressure and power generation in CGSs. Lo Cascio et al. [9] analyzed energy recovery systems in gas pressure reduction stations. They argued that the lack of performance indicators to highlight the importance and benefits of these systems was the reason for their lack of proper development. They provided a suitable indicator for energy recovery and reducing greenhouse gas emissions and environmental pollution. A model was also presented to predict key performance indicators based on system specifications. The obtained results were compared with the modeling performed for a station with a pressure ratio of 4.8 using UniSim software. Andrei et al. [10] examined the use of turboexpanders to recover energy in CGSs in Romania. The experiment was performed at an actual airflow rate of 26% and inlet pressure of 5.5 bar and the results were recorded and evaluated. Ashouri et al. [11] proposed a procedure for computation of Joule–Thomson coefficient using thermodynamic equations and AGA-8 equation of state to reduce the energy consumption of preheaters in gas pressure reduction stations and calculated the minimum inlet gas temperature to pressure relief valves without the formation of gas hydrates. The procedure was applied to a gas pressure reduction station with a capacity of 20,000 SCMH. The results showed the energy consumption reduced by 43% and the period of return was estimated to be less than a year for this project.

Jedlikowski et al. [12] studied energy consumption in gas pressure reduction stations in Poland. They examined a variety of renewable electric heating technologies for gas preheating and performed their analyses for three different weather conditions and two types of gas pressure reduction stations. The results showed that electric preheating by renewable sources reduced energy consumption by more than half as well as environmental pollution. Lo Cascio et al. [13] proposed a hybrid system, equipped with turboexpanders, linear parabolic solar collectors, and thermal energy storage, for preheating of gas pressure reduction stations using renewable energy to reduce energy consumption. The system performance was evaluated from energy and environmental perspectives by a dynamic model in MATLAB-Simulink programming and the rate of energy consumption was examined in three cities, namely Genoa, Naples, and Amsterdam. The results illustrated that the system could operate by only solar energy in the southern regions. Neseli et al. [14] studied a gas pressure reduction station equipped with turboexpanders in Marmara, Turkey. They analyzed energy and exergy efficiencies of the inlet and outlet flow of the station and its equipment over a period of time and calculated exergy efficiency and exergy degradation in turbines and heat exchangers. The mean energy and exergy

efficiencies of the station were 71.96% and 78.25%, respectively. Ghorbani et al. developed a hybrid solar-based multigeneration plant using a Kalina power generation cycle, flat plate collectors, and multi-effect desalination unit. The total energy and exergy efficiencies of the integrated structure were 44.04% and 90.04%, respectively.

Nami et al. [15] developed a hybrid power generation system consisting of a gas turbine, heat recovery system generator (HRSG), supercritical CO_2 recompression Brayton cycle, and organic Rankine cycle (ORC) and performed exergoeconomic and environmental analyses. The parameters affecting the exergoeconomic efficiency of the cycle were investigated. The optimization results showed the cost reduced by 0.56 \$/GJ compared to the base conditions. El Saie et al. [16] investigated a novel hybrid system consisting of a gas turbine, Rankine power cycle, and multistage desalination for a specific demand thermodynamically and economically. They examined three combinations of different component sizes and then selected the optimal model based on technical and economic parameters. Shakib et al. [17, 18] simulated a system consisting of a gas turbine, HRSG, and multistage evaporation desalination and analyzed it thermo-economically. They used an innovative optimization algorithm to optimize the system. The results revealed that the prime cost of the product reduced by 19% and the system exergy efficiency increased by 19%. Ghorbani et al. [19] developed novel integrated structures for the simultaneous production of liquefied natural gas, liquid CO_2, and freshwater using oxy-fuel power plant, multiple-effect distillation and two-stage refrigeration system. They used HYSYS software and MATLAB programming language for exergy analysis. Ghorbani et al. [20] investigated a novel integrated structure for trigeneration of power (309.1 MW), water (17.36 kg s^{-1}), and liquid carbon dioxide (88.4 kg s^{-1}) using oxy-fuel power plant, air separation unit, organic Rankine plant, regasification operation, and water desalination. The results illustrated the prime cost of the product and return period were 0.148 \$ kWh^{-1} and 3.1 years.

Calise et al. [21] examined a solar trigeneration (combined cooling, heat, and power) system consisting of an absorption chiller and multistage desalination. The system was simulated by TRNSYS software and the optimal values of the main parameters were calculated. Vakilabadi et al. [22] used parabolic trough collectors to supply inlet heat to the multistage Rankine cycle in California's the Mojave Desert. The results showed that the maximum exergy efficiency (32.7%) and maximum energy efficiency (23%) occurred at 12 noon.

Shaygan et al. [23] developed a novel integrated system for cogeneration of power and hydrogen using polymer electrolyte membrane fuel cell and photovoltaic cells. The results showed that the highest and lowest exergy destruction occurred in the photovoltaic cells (37.67 kW) and

compressor (3.7 kW), respectively. Ahmadi et al. [24] investigated a novel hybrid structure for cogeneration of power and hydrogen using a gas turbine, air bottoming cycle, and a reformer unit. the results illustrated that adding a heat recovery steam generator to the integrated structure improved the energy efficiency to 67.6% and the period of return to 0.41 years. Ehyaei et al. [25] used geothermal energy to supply inlet heat to a system combining an organic Rankine unit and an absorption chiller. Exergy and economic analyses were used to evaluate the integrated structure and the multi-objective particle swarm algorithm for optimization.

So far, many studies have been conducted to recover energy from natural gas pressure reduction stations for cogeneration of power and refrigeration. However, according to the literature review, no study has ever been performed on energy recovery from natural gas pressure reduction stations using integrated cogeneration structures exploiting natural gas with high efficiency and thermal integration. The present study focuses on energy recovery from natural gas pressure reduction stations to generate refrigeration using turboexpanders and compression refrigeration cycle. Also, the natural gas and compressed air combustion are carried out to generate power and freshwater using the integrated structures of Brayton power generation system, CO_2 power generation plant, Rankine power generation cycle,

and multi-effect thermal desalination unit. Thermal integration is employed to increase the efficiency of the integrated structure. Exergy and economic analyses are performed to investigate the second law of thermodynamics and the feasibility of the developed structure.

Process description

Normally, high-pressure natural gas (4–7 MPa) should reach a much lower pressure at points of the transmission pipeline in pressure reduction stations before being used by consumers. The pressure is usually dropped by expansion valves. As the gas passes through them, the pressure and temperature of the gas decrease at constant enthalpy by the Joule–Thomson effect. Therefore, most of the gas energy, which is compressed, is wasted. The use of turboexpanders, like expansion valves at the station, is a useful and reliable way to convert this huge amount of energy into electrical energy and refrigeration. Low-pressure natural gas can also be used to supply fuel in an integrated structure. Figure 1 shows the block diagram of the integrated structure for trigeneration of power, refrigeration, and freshwater in natural gas pressure reduction stations. This integrated structure generates 105.6 MW of power and 34.73 kg s^{-1} of freshwater by
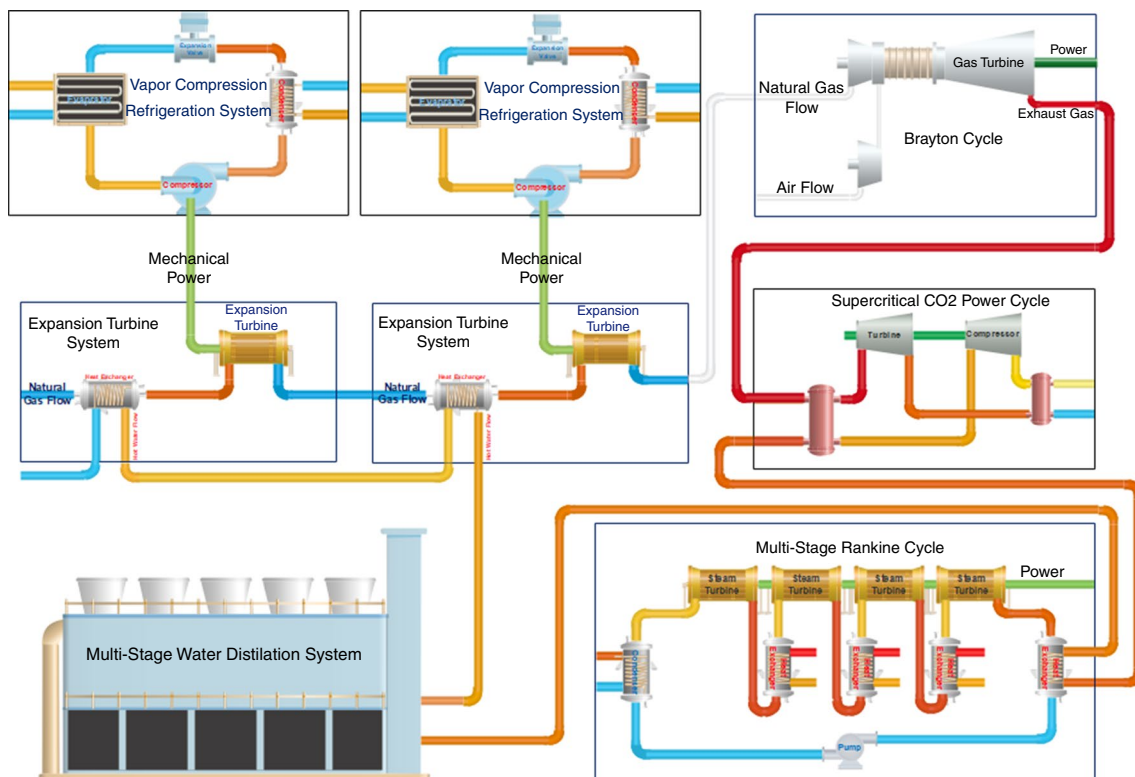
Fig. 1 Block diagram of the integrated structure for trigeneration of power, refrigeration, and freshwater in natural gas pressure reduction stations

reducing the gas pressure by 2.960 MW, burning natural gas and air in the combustion chamber, and applying waste heat. The HYSYS v10.0 software and MATLAB v10.0 programming language are used to simulate the developed integrated structure. Figure 2 presents the process diagram of turbo-expanders, compression refrigeration cycle, Bryton power generation system, CO_2 power generation plant, multistage Rankine cycle, and multi-effect thermal desalination unit. Natural gas with a pressure of 44.82 bar, the temperature of 29 °C, and flow rate of 1,000 kmol h^{-1} is the system fuel input. Table 1 shows the characteristics of the flows used in the integrated structure for trigeneration of power, refrigeration, and freshwater in natural gas pressure reduction stations.

After the temperature increased in the return flow, high-pressure natural gas flow (stream R40) with a temperature of 29 °C and pressure of 40 bar enters the T1 and T2 expanders, respectively, and its pressure decreases by 7 bar. The power generated by the expanders is used to supply the power of compressors in two compression refrigeration cycles. The waste energy of the natural gas pressure drop generates 2.960 MW of refrigeration. Then, natural gas and compressed airflow enter the constant pressure combustion chamber and the resulting combustion flow (stream R65) with a temperature of 1287 °C and pressure of 4 bar enters the T3 gas turbine and generates 82.86 MW of power. The output flow of the gas turbine enters the CO_2 power generation plant, Rankine power generation cycle, and thermal desalination unit, respectively. The carbon dioxide gas (stream R79) with a temperature of 558 °C and pressure of 250 bar increase up to 835 °C with heat absorption in the HX25 exchanger. High-temperature and high-pressure gas (stream R80) enters the T4 turbine and generates 45.23 MW of power. The output flow (stream R126) of the gas turbine enters The HX23 and HX22 exchangers to recover energy and is used to preheat the input flow to the boiler.

The output flow (stream R129) of the HX22 exchanger is divided into two parts. The two divided flows are mixed after the pressure increase in the compressors and enter the boiler (the HX25 exchanger) as stream R79 after heat recovery in the HX23 exchanger. The net power output and efficiency of the CO_2 power generation cycle are 20.64 MW and 41.20%, respectively. Then, the output gas flow (stream R78) of the CO_2 power generation cycle boiler with a temperature 598.1 °C and pressure of 1 bar is divided into two parts and enters the Rankine power cycle. Streams R82 and R81 enter the HX12 and HX13 exchangers, respectively, and are supplied the required heat by the Rankine power generation cycle. After increasing the pressure in the P2 pump by 186.3 bar and heat temperature in the return flow up to 196.5 °C, the water flow enters the HX13 exchanger, and its temperature increases to 542 °C. Then, high-pressure and high-temperature flow (stream R2) enters the T5 and T6 turbines, respectively, and its pressure reduces by 36 bar. A portion of the output flow of the T6 turbine enters the boiler as the return flow to supply heat and the rest goes to the second boiler (HX13 exchanger) and its output temperature increase to 536 °C and then enters other turbines. The net power output and efficiency of the CO_2 power generation cycle are 29.50 and 41.01%, respectively. A portion of the
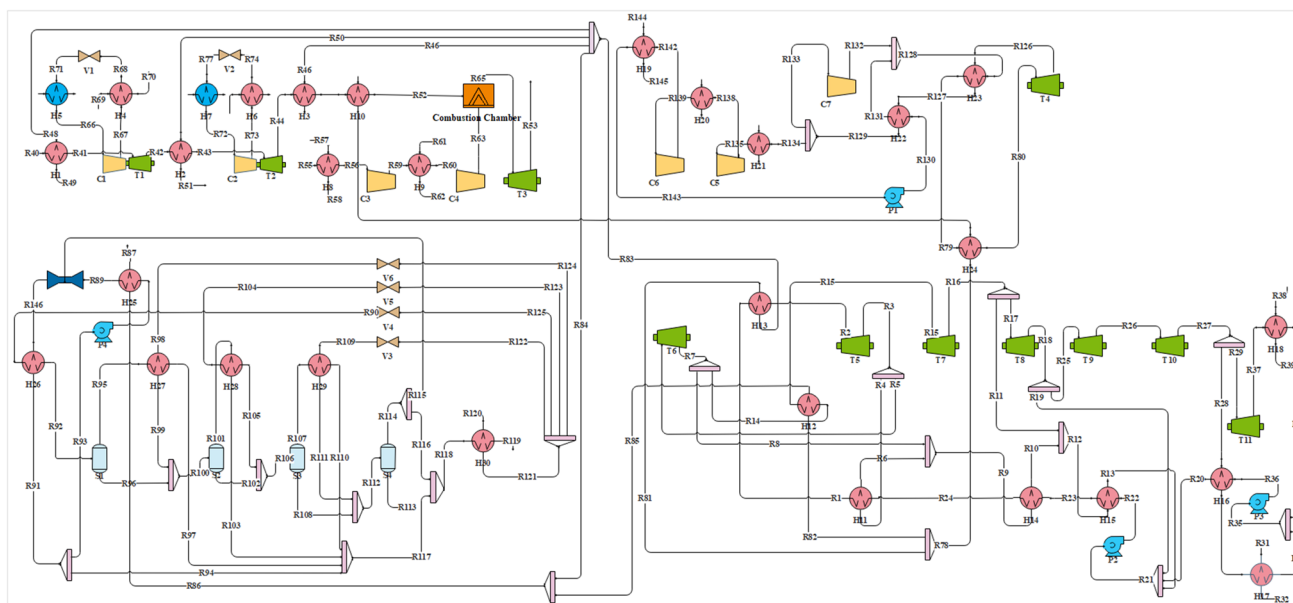

Fig. 2 Process diagram of the developed integrated structure for trigeneration of power, refrigeration, and freshwater in natural gas pressure reduction stations

Table 1 Characteristics of the streams used in the integrated structure for trigeneration of power, refrigeration, and freshwater in natural gas pressure reduction stations

Stream	Total exergy/ kW	Physical exergy/kW	Chemical exergy/kW	Molar enthalpy/ kJ kmol^{-1}	Molar entropy/ kJ kmol^{-1} $^{\circ}$C^{-1}	Molar flow/ kmol h^{-1}	Temperature/$^{\circ}$C	Pressure/ kPa	Mass flow/ kg s^{-1}
R1	19,969.0	4388.2	15,580.8	− 272,243.5	89.52	4789.99	196.48	18,600.0	23.97
R2	51,091.6	35,510.8	15,580.8	− 227,092.6	162.50	4789.99	542.00	18,600.0	23.97
R3	45,633.5	30,052.6	15,580.8	− 230,713.2	164.12	4789.99	404.65	7600.0	23.97
R6	246.2	90.4	155.8	− 263,700.7	106.45	47.90	289.00	7590.0	0.24
R7	41,132.9	25,707.9	15,425.0	− 233,405.5	165.39	4742.09	307.16	3600.0	23.73
R8	1234.0	771.2	462.8	− 233,405.5	165.39	142.26	307.16	3600.0	0.71
R9	1473.9	855.3	618.6	− 241,036.5	150.94	190.16	245.05	3600.0	0.95
R10	1349.4	730.8	618.6	− 246,577.8	140.26	190.16	244.89	3590.0	0.95
R15	46,620.7	31,658.5	14,962.3	− 224,125.5	178.86	4599.83	536.00	3600.0	23.02
R16	41,189.5	26,227.2	14,962.3	− 228,167.1	179.57	4599.83	423.40	1700.0	23.02
R17	39,541.9	25,178.1	14,363.8	− 228,167.1	179.57	4415.84	423.40	1700.0	22.10
R18	33,404.8	19,041.1	14,363.8	− 232,877.1	180.55	4415.84	289.42	600.0	22.10
R19	3146.3	1793.4	1352.9	− 232,877.1	180.55	415.92	289.42	600.0	2.08
R22	18,517.2	2936.4	15,580.8	− 275,477.5	82.33	4789.99	157.64	18,630.0	23.97
R23	19,705.6	4124.7	15,580.8	− 272,793.3	88.34	4789.99	190.00	18,620.0	23.97
R24	19,810.1	4229.3	15,580.8	− 272,573.3	88.81	4789.99	192.60	18,610.0	23.97
R25	30,258.5	17,247.6	13,010.9	− 232,877.1	180.55	3999.91	289.42	600.0	20.02
R26	29,848.4	16,837.5	13,010.9	− 233,214.0	180.66	3999.91	279.69	550.0	20.02
R29	23,443.3	11,473.3	11,970.0	− 236,835.0	181.69	3679.92	174.09	200.0	18.42
R30	1049.0	8.1	1040.9	− 284,119.8	60.44	319.99	52.00	190.0	1.60
R31	1002.9	0.2	1002.7	− 287,561.9	− 167.63	308.27	25.00	200.0	1.54
R34	12,005.1	35.1	11,970.0	− 284,900.4	58.02	3679.92	42.00	9.0	18.42
R37	14,790.4	2820.4	11,970.0	− 243,453.2	187.89	3679.92	46.01	10.0	18.42
R38	612,411.2	109.5	612,301.7	− 287,561.9	− 167.63	188,239.18	25.00	200.0	941.99
R41	236,370.3	2606.7	233,763.5	− 75,137.4	159.45	1000.00	80.00	4481.6	5.00
R42	235,693.6	1930.1	233,763.5	− 76,953.0	161.53	1000.00	25.63	1723.7	5.00
R43	235,785.5	2021.9	233,763.5	− 73,947.0	170.50	1000.00	100.00	1723.7	5.00
R49	194.9	2.1	192.8	− 41,544.3	156.16	354.43	38.84	100.0	2.79
R50	410.4	162.5	247.8	− 35,370.6	172.64	455.70	205.60	100.0	3.58
R51	248.4	0.5	247.8	− 41,967.1	154.80	455.70	36.65	100.0	3.58
R53	106,362.2	94,683.4	11,678.7	− 11,838.4	202.63	21,473.07	906.17	100.0	168.79
R54	96,124.9	84,446.2	11,678.7	− 14,158.1	200.60	21,473.07	840.70	100.0	168.79
R55	756.1	− 158.0	914.1	285.6	152.77	20,437.00	35.00	100.0	163.78
R62	37,458.0	480.9	36,977.1	− 283,558.6	62.17	11,367.81	60.00	100.0	56.89
R63	23,115.6	22,201.5	914.1	3312.9	149.71	20,437.00	137.65	400.0	163.78
R65	191,598.6	179,919.9	11,678.7	2054.0	201.29	21,473.07	1287.15	400.0	168.79
R66	21,014.1	482.2	20,531.8	− 897,388.2	191.27	461.87	18.00	500.0	13.09
R67	21,411.4	879.5	20,531.8	− 893,457.0	194.07	461.87	81.80	2000.0	13.09
R68	21,161.0	629.2	20,531.8	− 908,711.3	149.46	461.87	67.00	2000.0	13.09
R71	21,059.8	528.0	20,531.8	− 908,711.3	152.10	461.87	15.76	500.0	13.09
R72	21,800.6	500.3	21,300.3	− 897,388.2	191.27	479.16	18.00	500.0	13.58
R73	22,212.7	912.4	21,300.3	− 893,457.0	194.07	479.16	81.80	2000.0	13.58
R74	21,953.0	652.7	21,300.3	− 908,711.3	149.46	479.16	67.00	2000.0	13.58
R76	10,013.1	95.7	9917.4	− 283,958.6	60.96	3048.89	55.00	100.0	15.26
R77	21,848.0	547.7	21,300.3	− 908,711.3	152.10	479.16	15.76	500.0	13.58
R78	61,142.6	49,463.8	11,678.7	− 22,556.6	192.11	21,473.07	598.05	100.0	168.79
R79	143,138.3	78,101.4	65,036.9	− 370,051.7	170.89	11,606.55	558.02	25,090.0	141.89
R80	177,736.6	112,699.7	65,036.9	− 354,513.8	187.01	11,606.55	835.00	25,090.0	141.89

Table 1 (continued)

Stream	Total exergy/ kW	Physical exergy/kW	Chemical exergy/kW	Molar enthalpy/ kJ kmol^{-1}	Molar entropy/ kJ kmol^{-1} °C^{-1}	Molar flow/ kmol h^{-1}	Temperature/°C	Pressure/ kPa	Mass flow/ kg s^{-1}
R89	11,795.8	4145.8	7650.0	− 240,158.5	− 29.92	2351.82	75.00	33.0	11.77
R90	16,801.4	166.6	16,634.8	− 286,810.0	− 159.43	4988.49	56.01	29.9	25.66
R91	7816.7	81.6	7735.1	− 285,016.0	− 159.50	2377.98	56.38	15.2	11.90
R92	20,522.7	3887.9	16,634.8	− 265,381.6	− 96.57	4988.49	67.96	25.9	25.66
R93	7730.7	80.7	7650.0	− 285,016.0	− 159.50	2351.82	56.38	15.2	11.77
R95	11,312.0	3711.5	7600.5	− 240,391.6	− 28.60	2336.61	67.96	25.9	11.69
R96	9210.7	166.1	9044.5	− 287,400.6	− 156.47	2651.88	67.96	25.9	13.96
R97	7716.7	116.2	7600.5	− 284,483.6	− 157.90	2336.61	62.92	22.9	11.69
R98	16,801.3	166.5	16,634.8	− 286,810.0	− 159.43	4988.49	56.02	26.1	25.66
R99	20,140.9	3506.1	16,634.8	− 266,157.3	− 98.25	4988.49	64.51	22.1	25.66
R103	7540.0	97.3	7442.7	− 284,722.0	− 158.61	2288.12	59.99	19.1	11.45
R104	16,801.2	166.4	16,634.8	− 286,810.0	− 159.43	4988.49	56.02	22.7	25.66
R105	19,824.1	3189.3	16,634.8	− 266,528.9	− 98.73	4988.49	60.96	18.7	25.66
R106	38,353.6	3471.0	34,882.6	− 277,460.4	− 129.04	10,340.75	60.96	18.7	53.82
R110	10,249.4	2808.6	7440.8	− 240,972.3	− 26.19	2287.51	57.24	15.7	11.45
R111	16,822.6	187.8	16,634.8	− 286,649.8	− 158.95	4988.49	58.00	16.7	25.66
R112	44,630.3	543.4	44,086.9	− 287,436.6	− 158.45	13,041.73	58.64	16.7	68.03
R116	7.7	2.2	5.5	− 240,699.6	− 25.88	1.69	58.64	16.7	0.01
R117	25,537.6	2968.5	22,569.1	− 270,219.0	− 114.62	6938.39	56.58	15.2	34.72
R120	66,539.1	0.0	66,539.1	− 289,313.8	− 167.43	19,953.97	25.00	101.3	102.62
R121	67,213.2	674.1	66,539.1	− 286,810.0	− 159.44	19,953.97	56.00	97.3	102.62
R124	16,803.3	168.5	16,634.8	− 286,810.0	− 159.44	4988.49	56.00	97.3	25.66
R125	16,803.3	168.5	16,634.8	− 286,810.0	− 159.44	4988.49	56.00	97.3	25.66
R126	126,935.2	61,898.3	65,036.9	− 368,542.2	192.81	11,606.55	579.68	2386.0	141.89
R131	80,870.5	37,692.6	43,178.0	− 381,297.7	155.36	7705.59	353.95	25,100.0	94.20
R135	59,264.3	16,086.3	43,178.0	− 394,526.8	144.85	7705.59	31.90	2356.0	94.20
R137	74,471.5	81.4	74,390.1	− 285,557.1	55.93	22,869.67	35.00	90.0	114.44
R138	62,172.5	18,994.5	43,178.0	− 392,802.8	146.07	7705.59	83.10	4055.0	94.20
R139	61,630.7	18,452.7	43,178.0	− 395,417.2	138.15	7705.59	31.90	4045.0	94.20
R141	82,114.3	89.7	82,024.6	− 285,557.1	55.93	25,216.71	35.00	90.0	126.19
R142	64,778.0	21,600.0	43,178.0	− 393,566.0	139.43	7705.59	93.08	7692.0	94.20
R143	63,489.2	20,311.2	43,178.0	− 402,343.1	112.01	7705.59	30.80	7682.0	94.20

output flow (stream R86) of the Rankine power generation cycle enters the four-stage thermal desalination system. The studied thermal desalination procedure is the MED-TVC system. The hot gas flow (stream R86) with a temperature of 231.2 °C and pressure of 1 bar enters the HX25 exchanger and is provided the required heat of the input flow to the ejector.

Then, R89 vapor flow together with the vapor flow exiting from the last stage (stream R115) enter the ejector. The vapor flow exiting from the ejector enters the HX26 exchanger to supply heat to the first stage of the four-stage desalination. The temperature of seawater flow increase after increasing the temperature in the desalination condenser (HX30 exchanger) and after being divided by the number of stages, the pressure of desalination water, as feedwater, is regulated by throttling valves and sprayed on the evaporator tubes in each stage and, then, a portion of it evaporates when it reaches the boiling point. This four-stage thermal desalination structure generates 6940 kmol h^{-1} of freshwater by receiving 29.30 MW of heat. The energy balance equations for each of the equipment used in the integrated structure are obtained by a specific enthalpy value [20, 26]:

$$\sum_{in} \dot{m}_{in} h_{in} - \sum_{out} \dot{m}_{out} h_{out} - \dot{W} + \dot{Q} = 0 \tag{1}$$

Irrespective of the amount of heat loss in heat exchangers, the energy balance equations can be considered as follows [27]:

$$\dot{m}_{in,i}(h_{in1,i} - h_{in2,i}) = \dot{m}_{out,i}(h_{out1,i} - h_{out2,i}) \tag{2}$$
$$T_{in1,i} = T_{out1,i} + \Delta T_{in,HXi}$$

Isentropic efficiency is used to provide energy balance equations for equipment that consumes or generates power, such as pumps and turbines, which are presented in Eqs. (3) and (4), respectively [27]:

$$h_{out} = \frac{h_{out}^S - h_{in}}{\eta_s} + h_{in} \tag{3}$$

$$h_{out} = (h_{out}^S - h_{in})\eta_s + h_{in} \tag{4}$$

Equations (5) and (6) indicate energy balance and mass conservation in the mixer [28]:

$$\dot{m}_{in,1} h_{in,1} + \dot{m}_{in,2} h_{in,2} = \dot{m}_{out} h_{out} \tag{5}$$

$$\dot{m}_{in,1} + \dot{m}_{in,2} = \dot{m}_{out} \tag{6}$$

By combining Eqs. (5) and (6), the refrigerant enthalpy is obtained at the output [28]:

$$h_{out} = \frac{\dot{m}_{in,1} h_{in,1} + \dot{m}_{in,2} h_{in,2}}{\dot{m}_{in,1} + \dot{m}_{in,2}} \tag{7}$$

Equations (8) and (9) can also be used as energy balance and mass conservation in flash drums and separators [27]:

$$\dot{m}_{in} h_{in} = \dot{m}_{out,1} h_{out,1} + \dot{m}_{out,2} h_{out,2} \tag{8}$$

$$\dot{m}_{in} = \dot{m}_{out,1} + + \dot{m}_{out,2} \tag{9}$$

According to the first law of thermodynamics, the throttling process in throttling valves is a constant enthalpy process, so [27]:

$$h_{in} = h_{out} \tag{10}$$

Exergy analysis

Exergy analysis is an engineering tool used to study the thermodynamic properties of a process and determine the maximum efficiency that can be achieved from a given amount of input energy [29]. Exergy of an energy source is the maximum amount of work that can be obtained when the source reaches a dead state (at 25 °C and 1 atm) from its specific thermodynamic state during a process. In the absence of kinetic, potential, nuclear, electrical, and magnetic energies and surface tension effects, the total exergy rate of each flow is calculated as follows [30, 31]:

$$e = e^{ph} + e^{ch} \tag{11}$$

The physical exergy of the flow of a matter is obtained by the following equation [32]:

$$e^{ph} = (h - h_o) - T_o(s - s_o) \tag{12}$$

where h_o and s_o are the enthalpy and the entropy of the flow at ambient temperature and pressure.

The chemical exergy of the non-ideal mixture flow is obtained by the following equation [33, 34]:

$$e^{ch} = \sum (x_i e_i^\circ) + RT_o \sum x_i Ln x_i = \sum (x_i e_i^\circ) + G - \sum x_i G_i \tag{13}$$

The HYSYS software and MATLAB programming language are used to calculate the physical and chemical exergies of the flow. The exergy balance of each equipment can be presented as follows [35]:

$$Ex_i + Ex_{Qi} = Ex_o + Ex_{Qo} + W_{sh} + I \tag{14}$$

The latter equation is used to calculate the irreversibility or lost exergy, where Ex_i and Ex_o are the exergies of the input and output material flow, respectively, Ex_{Qi} and Ex_{Qo} are the exergies of the input and output energy flow, respectively, W_{sh} is the axial work done on/by the system and I is the irreversibility or lost exergy.

Table 2 illustretes equations needed for the exergy analysis of the equipment employed in developed integrated process.

Economic analysis of the annualized cost of system (ACS)

The annualized cost of system is selected as a method to assess the feasibility of the integrated structure and economic analysis. This method covers all the costs of a system including the annualized capital cost (C_{acap}), annualized replacement cost (C_{arep}), annualized maintenance cost (C_{amain}), and annualized operating cost (C_{aope}) [30, 36]. Equations of equipment cost are updated using the Marshal and Swift cost index. In the economic analysis of the proposed integrated structures, the annual inflation rate, the bank nominal interest rate, and the useful life of the project are assumed to be 17%, 20%, and 20 years, respectively, and the replacement cost is excluded.

$$Cost_{refrence\,year} = Cost_{orginal\,year} \frac{Cost\,index_{refrence\,cost\,year}}{Cost\,index_{orginal\,cost\,year}} \tag{15}$$

Table 2 Equations applied for the exergy analysis of the equipment employed in the hybrid system

Equipment	Exergy destruction	Exergy efficiency
Heat exchangers [42]	$\dot{X}_{des} = \sum(\dot{m}x)_{in} - \sum(\dot{m}x)_{out}$	$\eta_{ex} = 1 - \left(\frac{\sum\dot{m}\Delta x}{\sum\dot{m}\Delta h}\right)_{hot} + \left(\frac{\sum\dot{m}\Delta x}{\sum\dot{m}\Delta h}\right)_{cold}$
Compressors [43]	$\dot{X}_{des} = \dot{W} + \sum(\dot{m}x)_{in} - \sum(\dot{m}x)_{out}$	$\eta_{ex} = \frac{\sum(\dot{m}x)_{in} - \sum(\dot{m}x)_{out}}{\dot{W}}$
Turbines [44]	$\dot{X}_{des} = -\dot{W} + \sum(\dot{m}x)_{in} - \sum(\dot{m}x)_{out}$	$\eta_{ex} = \frac{\dot{W}}{\sum(\dot{m}x)_{in} - \sum(\dot{m}x)_{out}}$
Expansion valves [42]	$\dot{X}_{des} = \sum(\dot{m}x)_{in} - \sum(\dot{m}x)_{out}$	$\eta_{ex} = \frac{x_{out}^{\Delta T} - x_{in}^{\Delta T}}{x_{out}^{\Delta P} - x_{in}^{\Delta P}}$
Flash drums and reactor [42]	$\dot{X}_{des} = \sum(\dot{m}x)_{in} - \sum(\dot{m}x)_{out}$	$\eta_{ex} = \frac{\sum(\dot{m}x)_{out}}{\sum(\dot{m}x)_{in}}$
Pumps [45]	$\dot{X}_{des} = \dot{W} + \sum(\dot{m}x)_{in} - \sum(\dot{m}x)_{out}$	$\eta_{ex} = \frac{\sum(\dot{m}x)_{in} - \sum(\dot{m}x)_{out}}{\dot{W}}$
Cycle	$\dot{X}_{des} = \sum(\dot{m}x)_{in} - \sum(\dot{m}x)_{out}$	$\eta_{ex} = \frac{\sum(\dot{m}x)_{out}}{\sum(\dot{m}x)_{in}}$

$\dot{X}_{des}$ Exergy destruction rate η_{ex} : Exergy efficiency, $(\dot{m}.\dot{e})_{in}$ Rate of inlet exergy by streams to each component, $(\dot{m}.\dot{e})_{out}$ Rate of outlet exergy by streams from each component, and $\dot{m}$ Molar flow
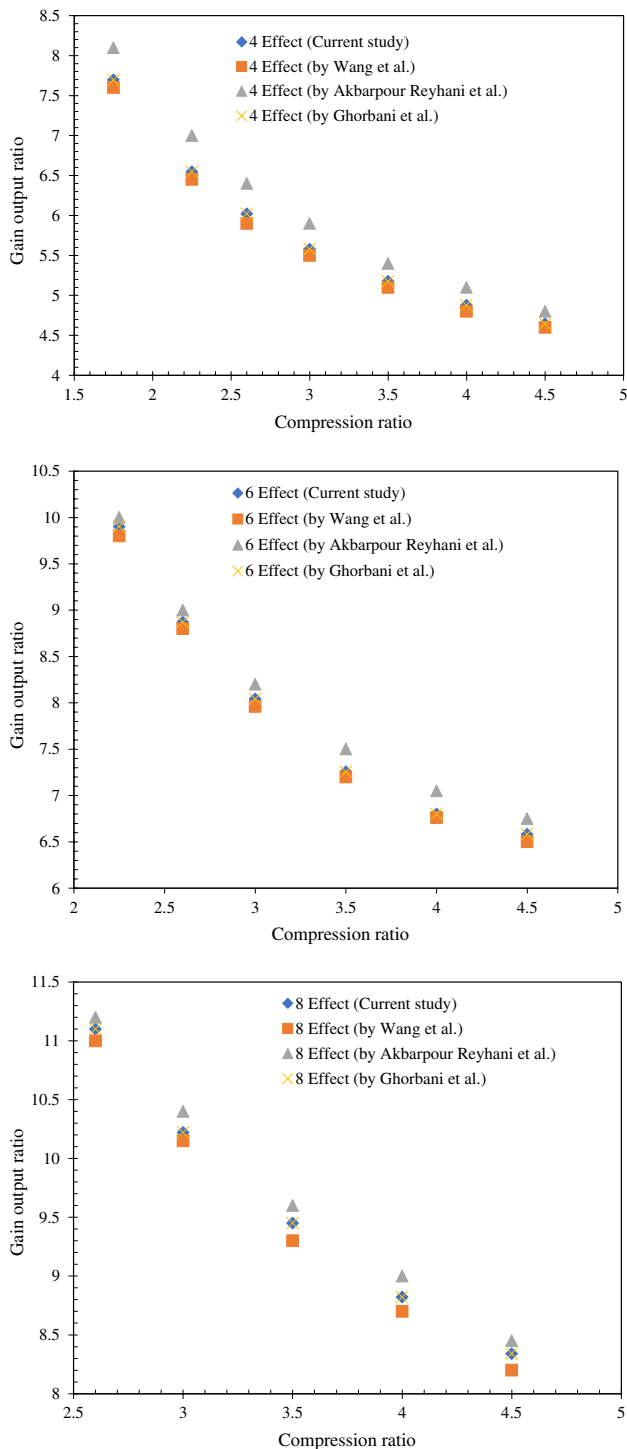
Results of energy, exergy, and economic analyses

Figure 3 illustrates the validity of the developed thermal desalination system based on the conditions mentioned in the reference papers [33, 37, 38]. The results of the validation of the developed desalination system show that increase compression ratio and the number of stages of thermal desalination increase the gain output ratio. After validation, the necessary changes are applied to observe industrial considerations in the cycle. Figure 4 shows the validation of the developed Rankine power generation cycle based on the reference papers [39–41]. The relative errors of the energy efficiency of the simulated cycle based on the reference papers of Piaderouhi et al. [39], and Ahmadi et al. [41] are 1.56% and 7.24%, respectively. This difference in relative error is due to the difference in input temperature to the power generation system reboiler.

Table 3 indicates the characteristics of input and output exergies, exergy degradation, and efficiency of each equipment used in the developed integrated structure. Among the heat exchangers used in the integrated structure, the HX5 exchanger with 99.66% has the highest exergy efficiency, and the HX25 exchanger with 85.81% has the lowest exergy efficiency. Also, the HX25 exchanger with 4156.3 kW has the highest rate of exergy degradation, and the HX17 exchanger with 4.127 kW has the lowest rate of degradation. Among the compressors of the integrated structure, the C3 compressor with 91.90% has the highest exergy efficiency, and the C1 and C2 compressors with 78.76% have the lowest exergy efficiency. Also, the C4 and C1 compressors with 15,389 kW and 107.07 kW have the highest and lowest rates of exergy degradation, respectively. Among the throttling valves of the integrated structure, the V6 valve with 86.31% has the highest exergy efficiency, and the V2 valve with 51.20%
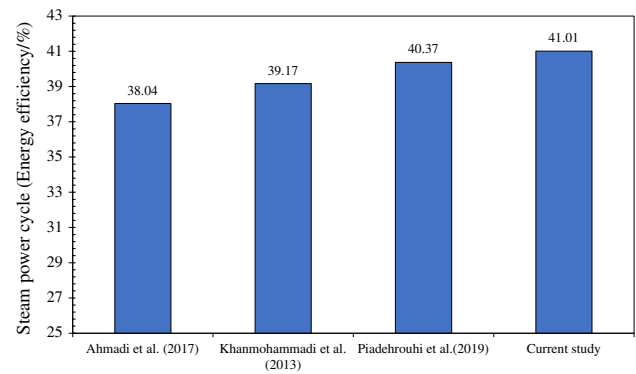
has the lowest exergy efficiency. Also, the V2 and V4 throttling valves with 105.03 kW and 1.867 kW have the highest and lowest rates of exergy degradation, respectively. Among the integrated structure turbines, the T3 turbine with 97.21% has the highest exergy efficiency, and the T1 turbine with 74.53% has the lowest exergy efficiency. Also, the T9 and T4 turbines with 35.68 kW and 5573 kW have the highest and lowest rates of exergy degradation, respectively. This integrated structure has an exergy efficiency and exergy degradation of 60.59% and 125,763.04 kW, respectively.

Figure 5 shows the exergy degradation rate of each equipment used in the integrated system for trigeneration of power, refrigeration, and freshwater. According to exergy analysis, the highest rates of exergy degradation are observed in the combustion chamber (59.67%), heat exchangers (14.70%), and compressors (14.45%), respectively. The two parameters of exergy degradation and efficiency of each equipment should be examined simultaneously to evaluate the exergy analysis of the integrated structure. Some equipment such as flash drums and valves may have lower exergy efficiency than other equipment, but their exergy degradation is relatively low. On the other hand, some equipment such as reactors and heat exchangers may have higher exergy degradation than other equipment, but instead, their exergy efficiency is high. Investigating the correlation between exergy efficiency and degradation of equipment allows the designer to re-examine the equipment. Given that the exergy degradation in compressors and turbines are directly associated with their power consumption and power output, respectively, this parameter in these components should be reduced as much as possible. Among the reasons for the high total exergy efficiency (60.59%) is the observance of the above points, so there is no need to reconsider the design of the integrated structure. Figure 6 shows the exergy degradation of heat exchangers used in the developed integrated structure.

Fig. 4 Validating the developed Rankine power generation cycle based on reference papers [39–41]

Fig. 3 Validating the developed thermal desalination system based on reference [33, 37, 38]

According to exergy analysis, the highest and lowest rates of exergy degradation in heat exchangers are observed in the HX25 and HX8 exchangers, respectively. The exergy efficiencies of the HX25 and HX8 exchangers are 85.81% and 99.59%, respectively.

Table 4 presents the cost analysis of the equipment used in the integrated trigeneration structure. Table 5 shows the economic analysis of the developed trigeneration structure. Table 6 indicates the results of the economic analysis using the ACS method to evaluate the developed integrated structure. The economic analysis of the integrated structure reveals that the period of return, additive value of product, the prime cost of product, and initial investment cost were 2.565 years, 0.1069 US\$ kWh^{-1}, 0.0430 US\$ kWh^{-1}, and 372.3 MMUS\$, respectively.

Figure 7 shows the changes in the prime cost of product and period of return with regard to the changes in electricity price in the developed integrated structure. With increasing electricity price, the period of return decrease, and the prime cost increase. The results show that the period of return in the developed integrated structure is less than 5 years and the prime cost is more than 0.038 US\$ kWh^{-1} for the electricity price of 0.092 US\$ kWh^{-1} and more.

Figure 8 shows the changes in the additive value of the product and annual net profit with regard to changes in electricity price in the developed integrated structure. With increasing electricity price, the additive value of the product and net annual benefit increase. The results indicate the additive value of the product and net annual benefit increase from 0.0167 to 0.3236 US\$ kWh^{-1} and 26.56 to 412.7 MMUS\$ Year^{-1}, respectively, by increasing electricity price from 0.05 to 0.039 US\$ kWh^{-1}.

Figure 9 illustrates the changes in the net annual benefit and period of return with regard to changes in the generated refrigeration cost in the developed integrated structure. As the generated refrigeration cost increased, the period of return decreases, and the net annual benefit increases. The results indicate the period of return is less than 2.68 years for different refrigeration costs, suggesting that refrigeration cost changes have no significant impact on the cost-effectiveness of the developed integrated structure compared to the electricity price.

Table 3 Exergy analysis of the equipment used in the integrated structure for trigeneration of power, refrigeration, and freshwater in natural gas pressure reduction stations

Equipment	Input exergy	Output exergy	Exergy destruction	Exergy efficiency
HX1	236,635.79	236,565.15	70.63	88.4
HX2	236,103.98	236,033.85	70.14	91.6
HX3	235,568.25	235,501.64	66.61	90.1
HX4	30,970.99	30,812.92	158.07	91.9
HX5	21,084.53	21,014.10	70.44	99.7
HX6	32,130.08	31,966.10	163.98	91.9
HX7	21,884.15	21,800.55	83.60	99.6
HX8	23,723.32	23,717.58	5.73	99.6
HX9	48,772.33	48,056.73	715.60	91.9
HX10	341,563.08	339,659.05	1904.03	86.2
HX11	20,266.48	20,215.24	51.24	88.3
HX12	52,983.38	52,739.56	243.83	97.9
HX13	68,027.08	66,290.68	1736.40	97.1
HX14	21,179.43	21,159.51	19.92	93.2
HX15	21,405.71	21,251.16	154.55	95.7
HX16	15,102.31	14,617.18	485.13	88.5
HX17	2051.91	2047.79	4.13	94.1
HX18	627,201.64	625,000.36	2201.28	94.8
HX19	340,153.09	339,166.31	986.79	94.7
HX20	144,196.87	143,745.03	451.84	91.9
HX21	134,175.15	133,735.86	439.29	91.3
HX22	172,310.12	170,922.06	1388.06	96.6
HX23	249,247.89	248,966.23	281.65	99.2
HX24	239,263.17	238,879.11	384.06	99.2
HX25	27,637.01	23,480.67	4156.34	85.8
HX26	28,339.33	27,767.77	571.56	98.1
HX27	28,113.33	27,857.63	255.69	99.1
HX28	27,620.21	27,364.10	256.11	99.1
HX29	27,347.07	27,071.93	275.14	96.5
HX30	92,084.30	91,246.08	838.22	94.0
T1	236,370.26	236,197.97	172.29	74.5
T2	235,785.46	235,620.31	165.15	76.0
T3	191,598.62	189,226.81	2371.81	97.2
T4	177,736.55	172,163.47	5573.09	89.0
T5	51,091.61	50,450.85	640.76	88.3
T6	45,177.12	44,679.29	497.83	87.7
T7	46,620.75	46,353.49	267.26	95.1
T8	39,541.90	39,182.16	359.74	94.1
T9	30,258.48	30,222.79	35.69	91.3
T10	29,848.39	29,505.08	343.31	92.1
T11	23,443.29	21,555.49	1887.80	78.2
C1	21,518.46	21,411.38	107.08	78.8
C2	22,323.79	22,212.70	111.08	78.8
C3	12,770.20	11,795.36	974.84	91.9
C4	25,987.99	10,598.78	15,389.21	81.3
C5	62,954.38	62,172.53	781.85	78.8
C6	65,593.24	64,778.02	815.23	85.3
P1	67,710.13	66,482.14	1227.99	70.9
P2	18,788.54	18,517.25	271.29	71.7
P3	13,062.90	13,063.77	−0.87	93.9
P4	13,049.35	13,063.77	14.42	76.1

Table 3 (continued)

Equipment	Input exergy	Output exergy	Exergy destruction	Exergy efficiency
S1	20,522.66	20,522.66	0.00	100.0
S2	29,350.58	29,350.59	-0.01	100.0
S3	38,353.58	38,353.59	-0.01	100.0
S4	44,630.31	44,630.32	-0.02	100.0
V1	21,161.05	21,059.80	101.24	59.2
V2	21,953.00	21,847.97	105.03	51.2
V3	16,803.29	16,801.17	2.12	73.7
V4	30,258.48	16,801.42	1.87	63.2
V5	16,803.29	16,801.22	2.07	73.2
V6	16,803.29	16,801.32	1.97	86.3
Reactor	266,649.77	191,598.62	75,051.15	71.9

Fig. 5 Exergy degradation rate of the equipment used in the developed integrated structure
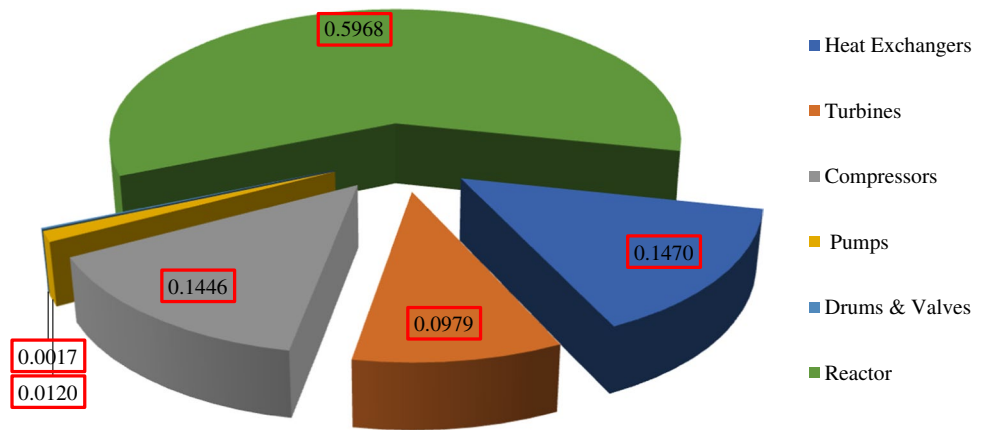
Fig. 6 Exergy degradation rate of heat exchangers used in the developed integrated structure
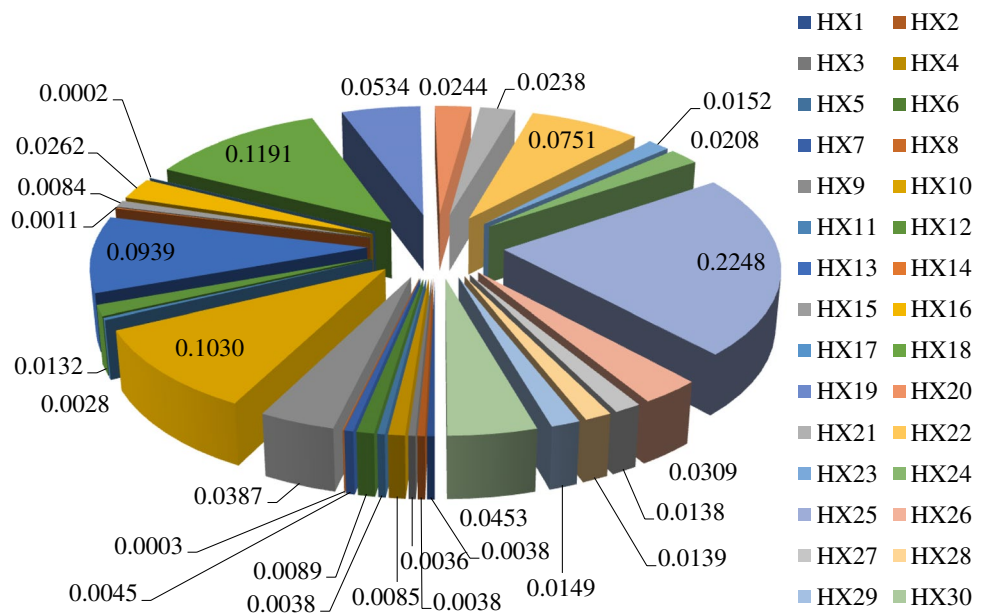
Figure 10 shows the changes in annual net profit and period of return with regard to changes in freshwater production cost in the developed integrated structure. As the freshwater production cost increases, the payback period decreases, and the annual net profit increases. The results indicated the period of return decrease from 2.65 to 2.45 years and the annual net profit

Table 4 Cost analysis of the equipment used in the integrated trigeneration structure [46–48]

Component	Purchased equipment cost functions
Gas turbine	$C_C = 7.90(\text{HP})^{0.62}$ C_C = Cost of Compressor (k\$)
Expander	$C_{Ex} = 0.378(\text{HP})^{0.81}$ C_{Ex} = Cost of Expander (k\$)
Condenser	$C_{condenser} = 516.621 \times A_{Condenser} + 268.45$
Steam turbine	$C_{ST} = 3644.3(\text{W})^{0.7} - 61.3(\text{W})^{0.95}$ C_{Ex} = Cost of Expander (k\$)
Pump	$C_P = f_M f_T C_b$ C_P = Cost of Pump (\$) $C_b = 1.39\exp[8.833 - 0.6019(\ln Q(H)^{0.5}) + 0.0519(\ln Q(H)^{0.5})^2]$, Q in gpm, H in ft head f_M = Material Factor $f_T = \exp[b_1 + b_2(\ln Q(H)^{0.5}) + b_3(\ln Q(H)^{0.5})^2]$ $b_1 = 5.1029$, $b_2 = -1.2217$, $b_3 = 0.0771$
Drum	$C_D = f_m C_b + C_a$ [95, 96] C_D = Cost of Drum (\$) $C_b = 1.218\exp[9.1 - 0.2889(\ln W) + 0.04576(\ln W)^2]$, $5000 < W < 226{,}000$ lb shell mass $C_a = 300 D^{0.7396} L^{0.7066}$, $6 < D < 10$, $12 < L < 20$ ft f_m = Material Factor
Cooler	$C_C = 1.218 \, k(1 + fd + fp)Q^{0.86}$, $20 < Q < 200$ M BTU hr^{-1} C_C = Cost of cooler (\$) f_m = Design Type f_P = Design Pressure (psi) $a = 0.4692$, $b = 0.1203$, $c = 0.0931$
Steam ejector	$C_{Ejector} = 16.14 \times 989 \, m_{vapor} (T_i/P_i)^{0.05} (P_e)^{-0.75}$ C_E = Cost of Steam Ejector (\$)
Heat exchanger MED	$C_{MED\,effects} = 430 \times 0.582 \, Q \, \Delta T_{LMTD}^{-1} \, dP_t^{-0.01} dP_s^{-0.1}$

increase from 140.3 to 149.7 MMUS\$ Year^{-1} by an increase in the freshwater production cost from 0.05 to 10 US\$ m^{-3}.

Figure 11 presents the changes in prime cost and payback period with regard to changes in investment cost in the developed integrated structure. With increasing investment cost, the prime cost of product and period of return increase. The results indicate the period of return is less than 5 years for the initial investment cost of 632.9 MMUS\$ and less, which was economically viable.

Figure 12 shows the changes in the additive value of product and net annual benefit with regard to changes in investment cost in the developed integrated structure. With increasing investment cost, the additive value of product and net annual benefit decrease. The results indicate the additive value of product and net annual benefit decrease from 0.1069 to 0.0324 US\$ kWh^{-1} and 140.3 to 46.55 MMUS\$ Year^{-1}, respectively, for an increase in the investment cost from 372.3 to 1861.5 US\$ kWh^{-1}.

Table 5 Economic analysis of the integrated trigeneration structure

| Definition	Parameter
Annualized cost of system	ACS = Cacap (Components) + Carep (Components) + Camain (Components) + Caope (Labor Cost + Fuel Cost + Insurance Cost) [48]
Annualized capital cost	Ccap = 1.1 of Total capital cost = 1.1 of (direct cost + Indirect cost + Other outlays) [48] $\text{Cacap} = \text{Ccap.CRF}(i, Yproj) = \text{Ccap}.\frac{i.(1+i)^{Yproj}}{(1+i)^{Yproj}-1}$ $i = \frac{j-f}{1-f}$ $j = 17, f = 20\%$
Annualized replacement cost	$\text{Crap} = \text{Ccap (In Base)}. (1+i)^{Yproj}$ [49] $\text{Carep} = \text{Crap.FSF}(I, Yproj) = \text{Crap}.\frac{j}{(1+i)^{Yproj}-1}$
Annualized maintenance cost	For Yproj = 20, Camain = 0.05 of Capital Cost
Annualized operating cost Operating flow cost	OFC = (Labor Cost + Fuel Cost + Insurance Cost) Number of labor = 50, Labor Cost = 400 US$ Month^{-1} Fuel Cost (Natural Gas Price) = 2 (US$ per Million Btu) Fuel Cost (Electrical Energy Price) = 0.1 (US$ kWh^{-1}) Insurance Cost = 0.02 of Capital Cost
Net present value	NPV = ACS/ CRF(i,Yproj)
I = Refrigeration price II = Freshwater price NEW ACS = ACS-I-II	II = Refrigeration Price = 0.043 (US$ kWh^{-1}) III = Freshwater Price = 0.5 (US$ m^{-3} Freshwater)
Levelized cost of Product Total Product in one Year (kWh Electrical Energy)	LCOP = NEW ACS/ Total Product in one Year
Prime cost	VOP = Volume of Product, PC = OFC/VOP
Summary of product cost	COP = Cost Of Product, SOPC = VOP. COP COP = 0.15 (US$ kWh^{-1})
Annual benefit	AB = SOPC- OFC
Net annual benefit	NAB = AB.(1-Tax percent), Tax = 0.1(AB)
Period of return	POR = Ccap/NAB
Rate Of Return	ROR = NAB/ Ccap
Additive Value	AV = COP − PC

Table 6 Results of economic analysis of the integrated trigeneration structure

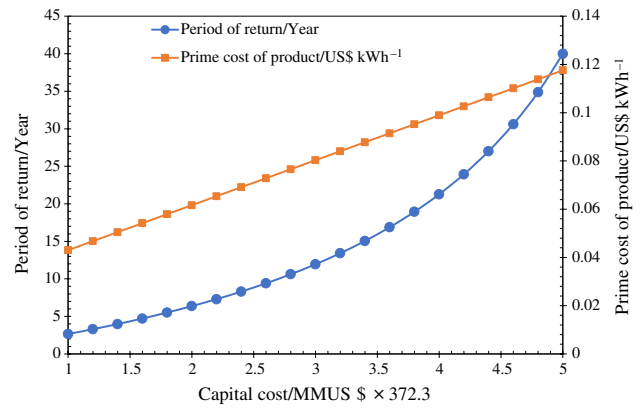| Parameter	Value
Capital Cost (MMUS$)	372.3
Electrical Energy Cost/MMUS$ Year^{-1}	136.1
Natural Gas Cost/MMUS$ Year^{-1}	13.40
Prime Cost of Product/US$ kWh^{-1}	0.0430
Net Annual Benefit/MMUS$ Year^{-1}	140.1
Annualized Operating Cost/MMUS$ Year^{-1}	60.12
Annualized Cost of System/MMUS$ Year^{-1}	84.15
Net Present Value/MMUS$ Year^{-1}	1303.9
Period of Return/Year	2.656
Rate of Return/Percent	37.63
Insurance Cost/MMUS$ Year^{-1}	7.446
Additive Value/US$ kWh^{-1}	0.1069
Annual Benefit/MMUS$ Year^{-1}	155.6
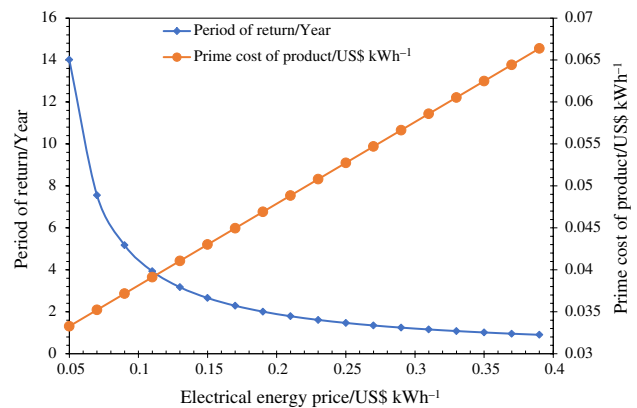
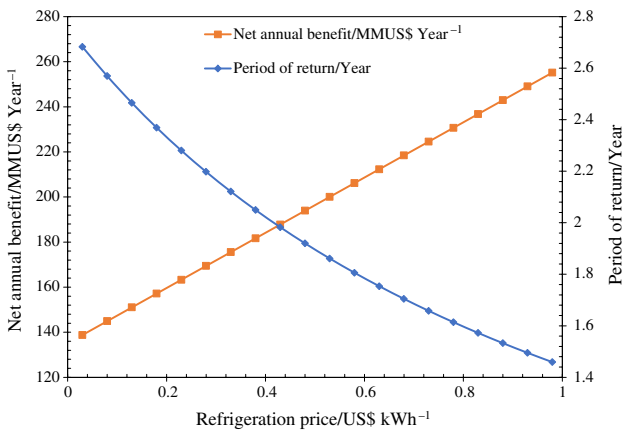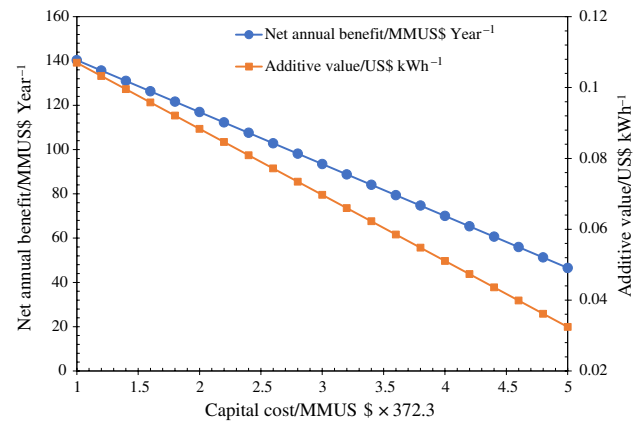**Fig. 7** Changes in prime cost and payback period with regard to changes in electricity price
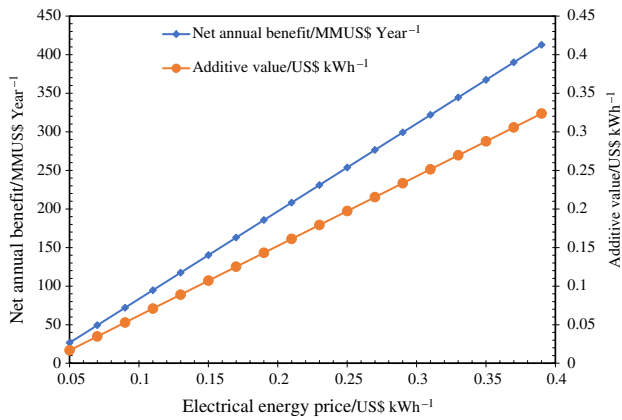
Fig. 8 The variation of the net annual benefit and the additive value versus the changes in electrical energy price
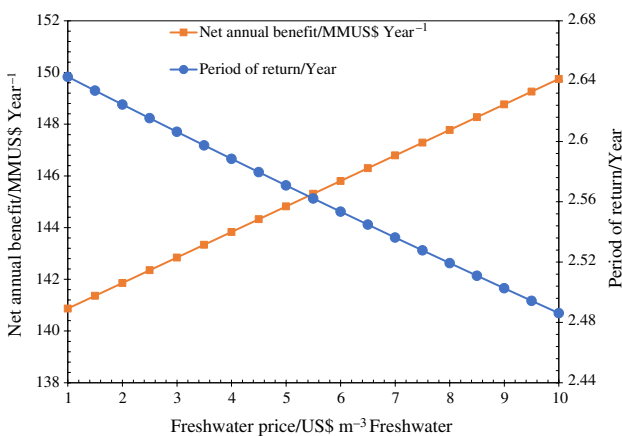

Fig. 9 Changes in net annual benefit and period of return with regard to changes in the generated refrigeration cost

Fig. 10 Changes of the net annual benefit and the period of return by increasing the freshwater production cost

Fig. 11 Changes of the prime cost and the period of return with regard to changes in capital cost

Fig. 12 Variation of the net annual benefit and additive value by increasing the Capital Cost

Conclusions

Exploiting gas pressure energy in transmission pipelines manifests the procedure of energy recovery. It is possible to prevent energy loss during the pressure regulation and reduction process by using turboexpanders at the end of the main gas pipelines in gas pressure reduction stations. These turbines are placed in the path of high-pressure gas flows to generate electrical power during the pressure reduction process. This study presented an integrated structure for the trigeneration of refrigeration, power, and freshwater through energy recovery from pressure reduction stations using the compression refrigeration cycle, Brayton power generation system, CO_2 power generation plant, Rankine power generation cycle, and multistage thermal desalination unit. The simulation results indicated the electrical and thermal efficiencies of the whole integrated structure were 47.04% and 61.42%, respectively. According to the exergy analysis of the integrated structure, the highest rates of

exergy degradation were observed in the combustion chamber (59.68%), heat exchangers (14.70%), and compressors (14.46%), respectively. The two parameters of exergy degradation and efficiency should be examined simultaneously to better compare the performance of different equipment in each process. As it is the purpose of exergy analysis, by comparing the exergy degradation and efficiency of various equipment in a process, the points at which the energy is not used efficiently can be found. Given that heat exchangers, turbines, and compressors had higher exergy efficiencies than other equipment, re-simulation is not required to modify the structure. Among the reasons for the high total exergy efficiency of the integrated structure (60.59%) was the proper design of the developed integrated structure. The results of the economic analysis using ACS revealed that the period of return, additive value, and annual benefit were 2.565 years, 0.1069 US$ kWh^{-1}, and 155.6 MMUS$, respectively. The parameters of electricity price, refrigeration cost, freshwater production cost, and capital cost were considered as the main design parameters in the sensitivity analysis. The sensitivity analysis of economic parameters showed that the period of return and prime cost of the product changed from 2.65 to 39.9 years and 0.043 to 0.1175 US$ kWh^{-1}, respectively, with an increase in the capital cost from 372.3 to 1861.5 MMUS$. Integration of integrated structures reduces equipment but makes the controllability of the integrated structure difficult. Dynamic investigation of the integrated structure can be investigated. It is recommended the advanced exergy and exergoeconomic analyses of the developed integrated structure be performed in future studies. Turboxpanders can also be used at the pressure reducing station to liquefy natural gas for peak shaving.

Author contributions Hooman Golchoobian contributed to methodology, investigation, software, validation, original draft, writing—original draft. Seyfolah Saedodin and Bahram Ghorbani contributed to supervision, conceptualization, methodology, investigation, software, validation, original draft, writing—original draft.

Compliance with ethical standards

Conflict of interest The author declares that he has no known competing financial interests or personal relationships that could have appeared to influence the work reported in this paper.

References

1. Farzaneh-Gord M, Faramarzi M, Ahmadi MH, Sadi M, Shamshirband S, Mosavi A, et al. Numerical simulation of pressure pulsation effects of a snubber in a CNG station for increasing measurement accuracy. Engineering Applications of Computational Fluid Mechanics. 2019;13(1):642–63.
2. Deymi-Dashtebayaz M, Dadpour D, Khadem J. Using the potential of energy losses in gas pressure reduction stations for producing power and fresh water. Desalination.497:114763.
3. Yao S, Zhang Y, Deng N, Yu X, Dong S. Performance research on a power generation system using twin-screw expanders for energy recovery at natural gas pressure reduction stations under off-design conditions. Appl Energy. 2019;236:1218–30.
4. Cascio EL, Von Friesen MP, Schenone C. Optimal retrofitting of natural gas pressure reduction stations for energy recovery. Energy. 2018;153:387–99.
5. Li C, Zheng S, Li J, Zeng Z. Optimal design and thermo-economic analysis of an integrated power generation system in natural gas pressure reduction stations. Energy Convers Manag. 2019;200:112079.
6. Pajączek K, Kostowski W, Stanek W. Natural gas liquefaction using the high-pressure potential in the gas transmission system. Energy. 2020;202:117726.
7. Golchoobian H, Taheri MH, Saedodin S. Thermodynamic analysis of turboexpander and gas turbine hybrid system for gas pressure reduction station of a power plant. Case StudTherm Eng. 2019;14:100488.
8. Diao A, Wang Y, Guo Y, Feng M. Development and application of screw expander in natural gas pressure energy recovery at city gas station. Appl Therm Eng. 2018;142:665–73.
9. Cascio EL, Borelli D, Devia F, Schenone C. Key performance indicators for integrated natural gas pressure reduction stations with energy recovery. Energy Convers Manag. 2018;164:219–29.
10. Andrei I, Valentin T, Cristina T, Niculae T. Recovery of wasted mechanical energy from the reduction of natural gas pressure. Procedia Eng. 2014;69:986–90.
11. Ashouri E, Veysi F, Shojaeizadeh E, Asadi M. The minimum gas temperature at the inlet of regulators in natural gas pressure reduction stations (CGS) for energy saving in water bath heaters. J Nat Gas Sci Eng. 2014;21:230–40.
12. Jedlikowski A, Englart S, Cepiński W, Badura M, Sayegh MA. Reducing energy consumption for electrical gas preheating processes. Therm Sci Eng Progress. 2020;19:100600.
13. Cascio EL, Ma Z, Schenone C. Performance assessment of a novel natural gas pressure reduction station equipped with parabolic trough solar collectors. Renew Energy. 2018;128:177–87.
14. Neseli MA, Ozgener O, Ozgener L. Thermo-mechanical exergy analysis of Marmara Eregli natural gas pressure reduction station (PRS): an application. Renew Sustain Energy Rev. 2017;77:80–8.
15. Nami H, Mahmoudi S, Nemati A. Exergy, economic and environmental impact assessment and optimization of a novel cogeneration system including a gas turbine, a supercritical CO2 and an organic Rankine cycle (GT-HRSG/SCO2). Appl Therm Eng. 2017;110:1315–30.
16. El Saie MA, El Saie YMA, El Gabry H. Techno-economic study for combined cycle power generation with desalination plants at Sharm El Sheikh. Desalination. 2003;153(1–3):191–8.
17. Shakib SE, Amidpour M, Aghanajafi C. Simulation and optimization of multi effect desalination coupled to a gas turbine plant with HRSG consideration. Desalination. 2012;285:366–76.
18. Shakib SE, Hosseini SR, Amidpour M, Aghanajafi C. Multi-objective optimization of a cogeneration plant for supplying given amount of power and fresh water. Desalination. 2012;286:225–34.
19. Ghorbani B, Mehrpooya M, Ghasemzadeh H. Investigation of a hybrid water desalination, oxy-fuel power generation and CO2 liquefaction process. Energy. 2018;158:1105–19.
20. Ghorbani B, Miansari M, Zendehboudi S, Hamedi M-H. Exergetic and economic evaluation of carbon dioxide liquefaction process in a hybridized system of water desalination, power generation,

and liquefied natural gas regasification. Energy Convers Manag. 2020;205:112374.

21. Calise F, d'Accadia MD, Piacentino A. A novel solar trigeneration system integrating PVT (photovoltaic/thermal collectors) and SW (seawater) desalination: dynamic simulation and economic assessment. Energy. 2014;67:129–48.

22. Vakilabadi MA, Bidi M, Najafi A, Ahmadi MH. Exergy analysis of a hybrid solar-fossil fuel power plant. Energy Sci Eng. 2019;7(1):146–61.

23. Shaygan M, Ehyaei M, Ahmadi A, Assad MEH, Silveira JL. Energy, exergy, advanced exergy and economic analyses of hybrid polymer electrolyte membrane (PEM) fuel cell and photovoltaic cells to produce hydrogen and electricity. J Clean Prod. 2019;234:1082–93.

24. Ahmadi A, Jamali D, Ehyaei M, Assad MEH. Energy, exergy, economic and exergoenvironmental analyses of gas and air bottoming cycles for production of electricity and hydrogen with gas reformer. J Clean Prod. 2020;259:120915.

25. Ehyaei M, Ahmadi A, Assad MEH, Rosen MA. Investigation of an integrated system combining an organic rankine cycle and absorption chiller driven by geothermal energy: energy, exergy, and economic analyses and optimization. J Clean Prod. 2020;258:120780.

26. Javadi MA, Ahmadi MH, Khalaji M. Exergetic, economic, and environmental analyses of combined cooling and power plants with parabolic solar collector. Environ Progress Sustain Energy. 2020;39(2):e13322.

27. Ghorbani B, Javadi Z, Zendehboudi S, Amidpour M. Energy, exergy, and economic analyses of a new integrated system for generation of power and liquid fuels using liquefied natural gas regasification and solar collectors. Energy Convers Manag. 2020;219:112915.

28. Amidpour M, Hamedi M, Mafi M, Ghorbani B, Shirmohammadi R, Salimi M. Sensitivity analysis, economic optimization, and configuration design of mixed refrigerant cycles by NLP techniques. J Nat Gas Sci Eng. 2015;24:144–55.

29. Ahmadi MH, Banihashem SA, Ghazvini M, Sadeghzadeh M. Thermo-economic and exergy assessment and optimization of performance of a hydrogen production system by using geothermal energy. Energy Environ. 2018;29(8):1373–92.

30. Mirzaei M, Ahmadi MH, Mobin M, Nazari MA, Alayi R. Energy, exergy and economics analysis of an ORC working with several fluids and utilizes smelting furnace gases as heat source. Thermal Science and Engineering Progress. 2018;5:230–7.

31. Ashouri M, Ahmadi MH, Pourkiaei SM, Astaraei FR, Ghasempour R, Ming T, et al. Exergy and exergo-economic analysis and optimization of a solar double pressure organic Rankine cycle. Therm Sci Eng Progress. 2018;6:72–86.

32. Noroozian A, Mohammadi A, Bidi M, Ahmadi MH. Energy, exergy and economic analyses of a novel system to recover waste heat and water in steam power plants. Energy Convers Manage. 2017;144:351–60.

33. Ghorbani B, Shirmohammadi R, Amidpour M, Inzoli F, Rocco M. Design and thermoeconomic analysis of a multi-effect desalination unit equipped with a cryogenic refrigeration system. Energy Convers Manag. 2019;202:112208.

34. Ghorbani B, Ebrahimi A, Moradi M, Ziabasharhagh M. Energy, exergy and sensitivity analyses of a novel hybrid structure for generation of Bio-Liquefied natural Gas, desalinated water and power using solar photovoltaic and geothermal source. Energy Convers Manag. 2020;222:113215.

35. Ahmadi M, Sadaghiani M, Pourfayaz F, Ghazvini M, Mahian O, Mehrpooya M, et al. Energy and exergy analyses of a solid oxide fuel cell-gas turbine-organic Rankine cycle power plant with liquefied natural gas as heat sink. Entropy. 2018;20(7):484.

36. Ebrahimi A, Ghorbani B, Lohrasbi H, Ziabasharhagh M. Novel integrated structure using solar parabolic dish collectors for liquid nitrogen production on offshore gas platforms (exergy and economic analysis). Sustain Energy Technol Assessments. 2020;37:100606.

37. Reyhani HA, Meratizaman M, Ebrahimi A, Pourali O, Amidpour M. Thermodynamic and economic optimization of SOFC-GT and its cogeneration opportunities using generated syngas from heavy fuel oil gasification. Energy. 2016;107:141–64.

38. Wang Y, Lior N. Performance analysis of combined humidified gas turbine power generation and multi-effect thermal vapor compression desalination systems—Part 1: The desalination unit and its combination with a steam-injected gas turbine power system. Desalination. 2006;196(1–3):84–104.

39. Piadehrouhi F, Ghorbani B, Miansari M, Mehrpooya M. Development of a new integrated structure for simultaneous generation of power and liquid carbon dioxide using solar dish collectors. Energy. 2019;179:938–59.

40. Khanmohammadi S, Azimian AR, Khanmohammadi S. Exergy and exergo–economic evaluation of Isfahan steam power plant. Int J Exergy. 2013;12(2):249–72.

41. Ahmadi G, Toghraie D, Akbari OA. Solar parallel feed water heating repowering of a steam power plant: A case study in Iran. Renew Sustain Energy Rev. 2017;77:474–85.

42. Mehrpooya M, Ghorbani B, Sadeghzadeh M. Hybrid solar parabolic dish power plant and high-temperature phase change material energy storage system. Int J Energy Res. 2019;43(10):5405–20.

43. Mohammadi A, Ashouri M, Ahmadi MH, Bidi M, Sadeghzadeh M, Ming T. Thermoeconomic analysis and multiobjective optimization of a combined gas turbine, steam, and organic Rankine cycle. Energy Sci Eng. 2018;6(5):506–22.

44. Mohammadi A, Ahmadi MH, Bidi M, Ghazvini M, Ming T. Exergy and economic analyses of replacing feedwater heaters in a Rankine cycle with parabolic trough collectors. Energy Rep. 2018;4:243–51.

45. Ahmadi MH, Alhuyi Nazari M, Sadeghzadeh M, Pourfayaz F, Ghazvini M, Ming T, et al. Thermodynamic and economic analysis of performance evaluation of all the thermal power plants: A review. Energy Sci Eng. 2019;7(1):30–65.

46. Mehrpooya M, Ghorbani B. Introducing a hybrid oxy-fuel power generation and natural gas/carbon dioxide liquefaction process with thermodynamic and economic analysis. J Clean Prod. 2018;204:1016–33.

47. Mehrpooya M, Taromi M, Ghorbani B. Thermo-economic assessment and retrofitting of an existing electrical power plant with solar energy under different operational modes and part load conditions. Energy Rep. 2019;5:1137–50.

48. Nouri M, Miansari M, Ghorbani B. Exergy and economic analyses of a novel hybrid structure for simultaneous production of liquid hydrogen and carbon dioxide using photovoltaic and electrolyzer systems. J Clean Prod. 2020;259:120862.

49. Niasar MS, Ghorbani B, Amidpour M, Hayati R. Developing a hybrid integrated structure of natural gas conversion to liquid fuels, absorption refrigeration cycle and multi effect desalination (exergy and economic analysis). Energy. 2019;189:116162.